Electronic Supplementary Information

Red to Blue OLEDs based on highly luminescent 1,3-bis(4-phenylpyridin-2-yl)-4,6-difluorobenzene platinum(II) complexes: the key role of substituents on the 4-phenylpyridine unit

In memoriam of Bertrand Carboni

Francesco Fagnani,[a] Alessia Colombo,[a,*] Giulia De Soricellis,[a, b] Claudia Dragonetti,[a] Dominique Roberto,[a] Daniele Marinotto,[c] Véronique Guerchais,[d] Francesca Tinti[e] and Massimo Cocchi[e]

[a] Dipartimento di Chimica dell'Università degli Studi di Milano and UdR-INSTM di Milano,Via C. Golgi 19, I-20133 Milan, Italy. E-mail: alessia.colombo@unimi.it

[b] Dipartimento di Chimica, Università di Pavia, Via Taramelli 12, 27100 Pavia, Italy.

[c] Istituto di Scienze e Tecnologie Chimiche (SCITEC) "Giulio Natta", Consiglio Nazionale delle Ricerche (CNR), via C. Golgi 19, I-20133 Milan, Italy

[d] Université de Rennes 1, CNRS, ISCR (Institut des Sciences Chimiques de Rennes) - UMR 6226, F-35000 Rennes, France.

[e] Istituto per la Sintesi Organica e la Fotoreattività (ISOF), Consiglio Nazionale delle Ricerche (CNR), via P. Gobetti 101, 40129 Bologna, Italy.

1. Synthesis of the Pt(II) complexes

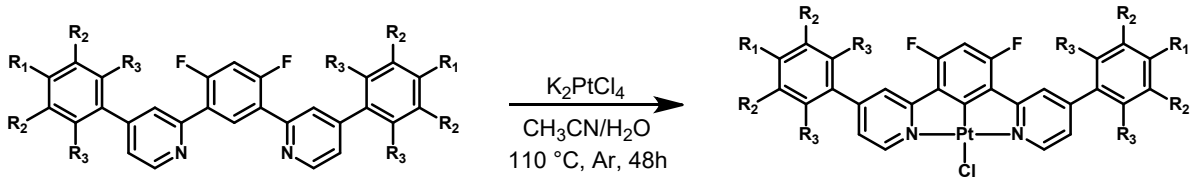

HL^n **PtL^{n}Cl**

PtL^{1}Cl : $R_1 = R_2 = R_3 = H$	**PtL^{4}Cl** : $R_1 = R_3 = H$, $R_2 = t$Bu
PtL^{2}Cl : $R_1 = NPh_2$, $R_2 = R_3 = H$	**PtL^{5}Cl** : $R_1 = R_3 = CH_3$, $R_2 = H$
PtL^{3}Cl : $R_1 = t$Bu, $R_2 = R_3 = H$	**PtL^{6}Cl** : $R_1 = OCH_3$, $R_2 = H$, $R_3 = CH_3$

Figure S1. General synthesis of complexes **PtL^{1}Cl-PtL^{6}Cl**.

General procedure for the synthesis of complexes PtL^{n}Cl [43-46]

HL^n (0.10 mmol) and K_2PtCl_4 (0.12 mmol) were added to a Schlenk tube together with a 9:1 mixture of CH_3CN (5.4 mL) and H_2O (0.6 mL), and the reaction mixture was heated at reflux under argon atmosphere. After 48 h the reaction was cooled to rt and the presence of a precipitate was observed; water was added to precipitate all the product, which was filtered on a Buchner funnel and washed with water, methanol and diethyl ether, obtaining an orange powder.

Complex PtL^{1}Cl – Yield: 93%

^{1}H-NMR (300 MHz, $CDCl_3$, δ): 9.32 (d, J = 6.1 Hz, $^3J(^{195}Pt)$ = 41 Hz, 2H), 8.11 (s, 2H), 7.69 – 7.78 (m, 4H), 7.58 (dd, J = 8.9, 5.0 Hz, 6H), 7.49 (dd, J = 6.0, 1.9 Hz, 2H), 6.77 (t, J = 11.3 Hz, 1H).

$^{19}F\{^1H\}$-NMR (282.36 MHz, $CDCl_3$, δ): -108.30 (s, $^3J(^{195}Pt)$ = 43.2 Hz, 2F).

$^{13}C\{^1H\}$-NMR (75.48 MHz, $CDCl_3$, δ): 151.8, 136.7, 130.3, 129.4, 127.2, 120.7, 120.4

Complex PtL^{2}Cl – Yield: 82%

^{1}H-NMR (300 MHz, $CDCl_3$, δ): 9.28 (d, J = 6.4 Hz, $^3J(^{195}Pt)$ = 44 Hz, 2H), 8.10 (s, 2H), 7.64-7.61 (m, 4H), 7.45 (dd, J = 2.2, J = 4.2 Hz, 2H), 7.38-7.31 (m, 8H), 7.22-7.10 (m, 16H), 6.77 (t, $^3J(^{19}F)$ = 11.3 Hz, 1H).

$^{19}F\{^1H\}$-NMR (282.36 MHz, $CDCl_3$, δ): -108.99 (s, 2F).

It was not possible to record a ^{13}C-NMR spectrum due to the very low solubility, both in $CDCl_3$ and DMSO-d_6.

Complex PtL^{3}Cl – Yield: 41%

^{1}H-NMR (300 MHz, $CDCl_3$, δ): 9.27 (d, J = 5.9 Hz, $^3J(^{195}Pt)$ = 39.3 Hz, 2H), 8.10 (s, 2H), 7.69 (d, J = 8.3 Hz, 4H), 7.58 (d, J = 8.3 Hz, 4H), 7.46 (dd, J = 5.9, 1.9 Hz, 2H), 6.73 (t, J = 11.2 Hz, 1H), 1.41 (s, 18H).

$^{13}C\{^1H\}$-NMR (75.48 MHz, $CDCl_3$, δ): 153.7, 151.7, 133.6, 126.7, 126.3, 120.3, 34.7, 31.1, 27.1.

$^{19}F\{^1H\}$-NMR (282.36 MHz, $CDCl_3$, δ): -109.00 (s, 2F).

Complex PtL^{4}Cl – Yield: 85%

^{1}H-NMR (300 MHz, $CDCl_3$, δ): 9.34 (d, J = 6.0 Hz, $^3J(^{195}Pt)$ = 39.4 Hz, 2H), 8.13 (s, 2H), 7.63 (s, 2H), 7.45-7.59 (m, 6H), 6.74 (t, J = 11.2 Hz, 1H), 1.43 (s, 36H).

$^{13}C\{^1H\}$-NMR (75.48 MHz, $CDCl_3$, δ): 164.3, 153.3, 152.0, 151.7, 136.6, 124.5, 121.5, 121.1, 35.2, 31.4.

$^{19}F\{^1H\}$-NMR (282 MHz, $CDCl_3$, δ): -108.48 (s, 2F).

Complex PtL^{5}Cl – Yield: 30%

^{1}H-NMR (300 MHz, $CDCl_3$, δ): 9.42 (d, J = 5.9 Hz, $^3J(^{195}Pt)$ = 40.4 Hz, 2H), 7.81-7.76 (m, 2H), 7.17 (dd, J = 1.9 and 4.0 Hz, 2H), 7.03 (s, 4H), 6.73 (t, J = 11.2 Hz, 1H), 2.38 (s, 6H), 2.11 (s, 12H).

$^{13}C\{^1H\}$-NMR (75.48 MHz, $CDCl_3$, δ): 164.3, 154.1, 151.9, 138.4, 135.1, 134.8, 128.7, 124.5, 123.7, 99.4, 29.7, 21.1, 20.6.

$^{19}F\{^1H\}$-NMR (282.36 MHz, $CDCl_3$, δ): -107.90 (s, $^4J(^{195}Pt)$ = 54.4 Hz, 2F).

Complex PtL^{6}Cl – Yield: 81%

^{1}H-NMR (300 MHz, $CDCl_3$, δ): 9.40 (d, J = 5.9 Hz, $^3J(^{195}Pt)$ = 40.2 Hz, 2H), 7.76 (s, 2H), 7.17 (d, J = 5.8, 2H), 6.68–6.80 (m, 5H), 3.87 (s, 6H), 2.13 (s, 12H).

$^{13}C\{^1H\}$-NMR (75.48 MHz, $CDCl_3$, δ): 164.2, 159.4, 153.8, 151.9, 136.3, 130.7, 124.9, 124.1, 113.3, 55.2, 21.2.

$^{19}F\{^1H\}$-NMR (282 MHz, $CDCl_3$, δ): -108.10 (s, 2F).

2. NMR spectra

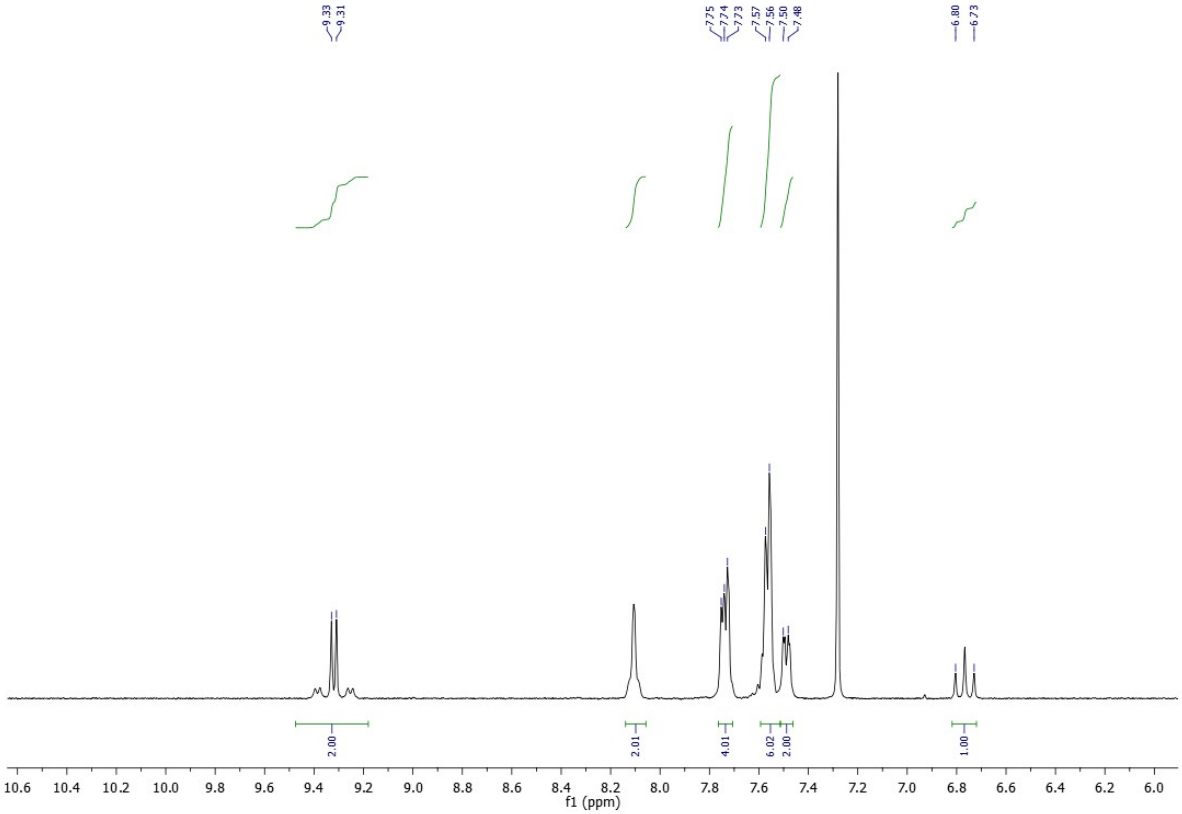

Figure S2. ^{1}H spectrum (300 MHz, $CDCl_3$) of **PtL^{1}Cl**.

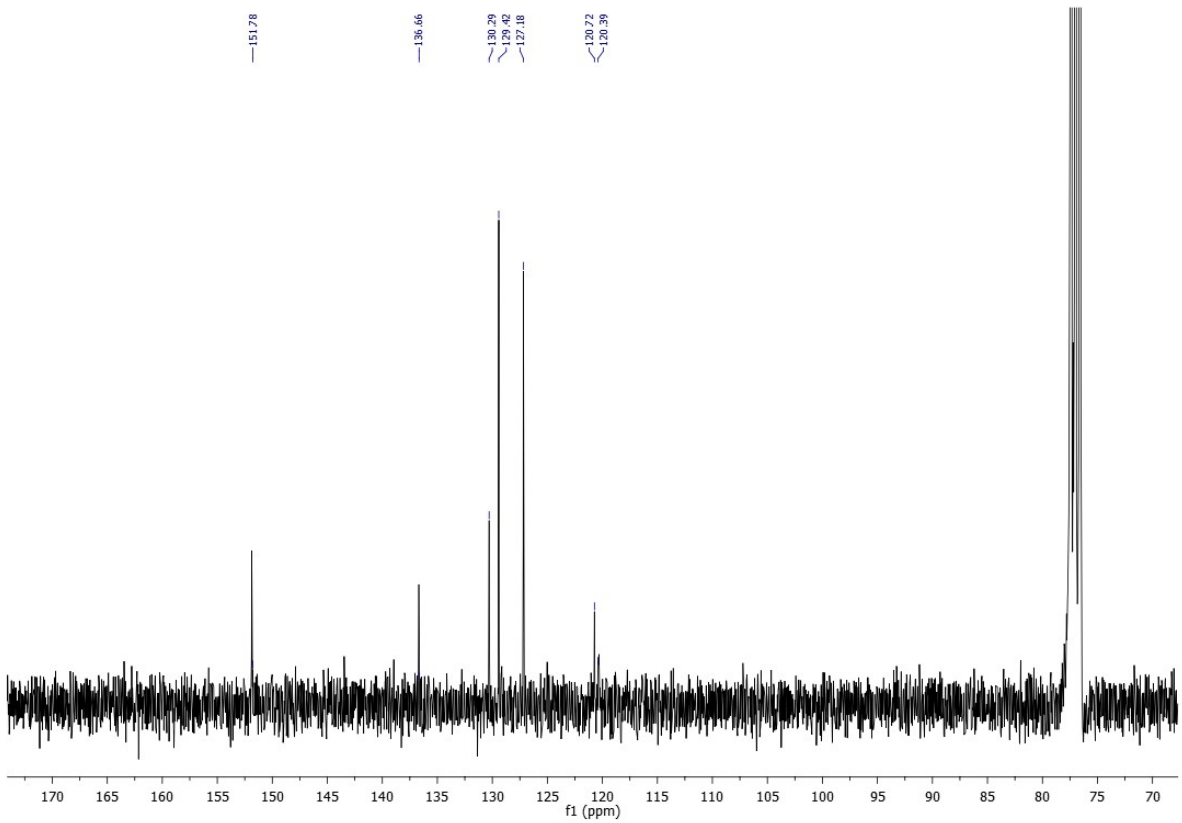

Figure S3. $^{13}C\{^{1}H\}$ spectrum (75.48 MHz, $CDCl_3$) of **PtL^{1}Cl**.

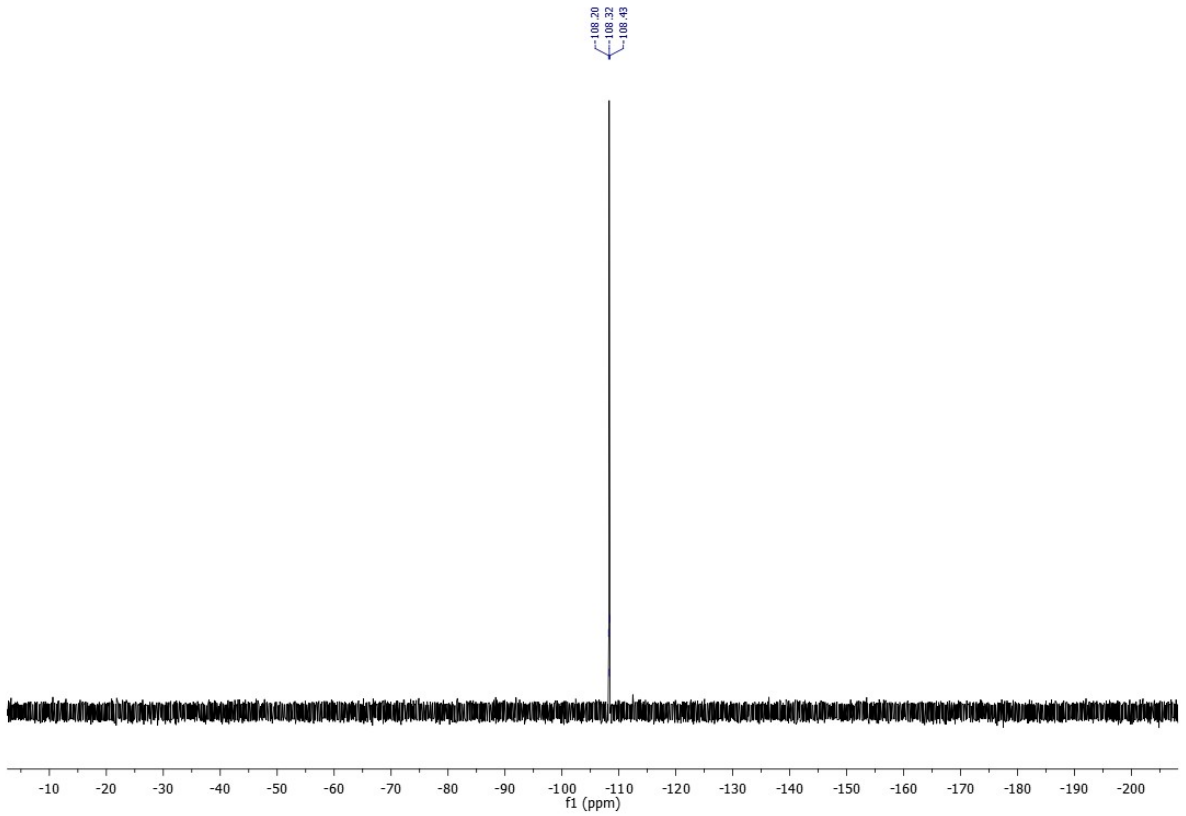

Figure S4. $^{19}F\{^{1}H\}$ spectrum (282.36 MHz, $CDCl_3$) of **PtL^{1}Cl**.

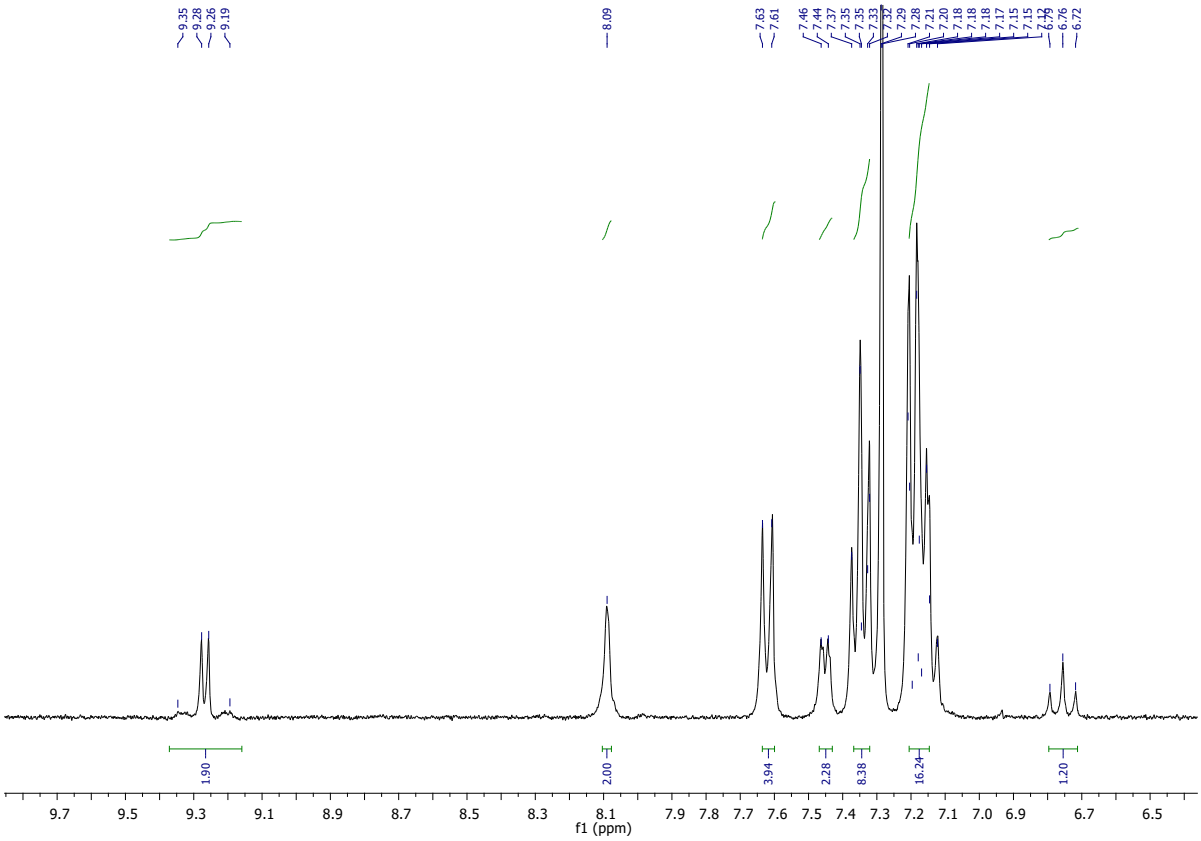

Figure S5. ^{1}H spectrum (300 MHz, $CDCl_3$) of **PtL^{2}Cl**.

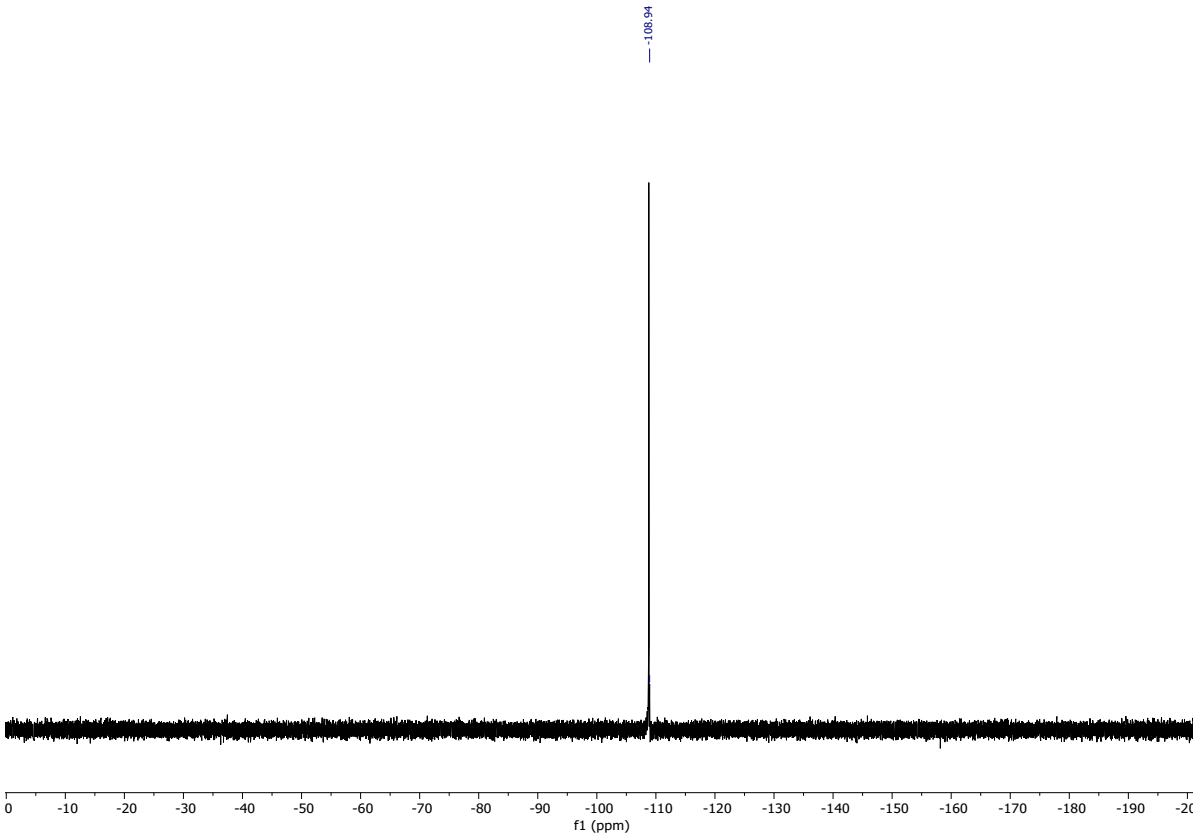

Figure S6. $^{19}F\{^{1}H\}$ spectrum (282.36 MHz, $CDCl_3$) of **PtL^{2}Cl**.

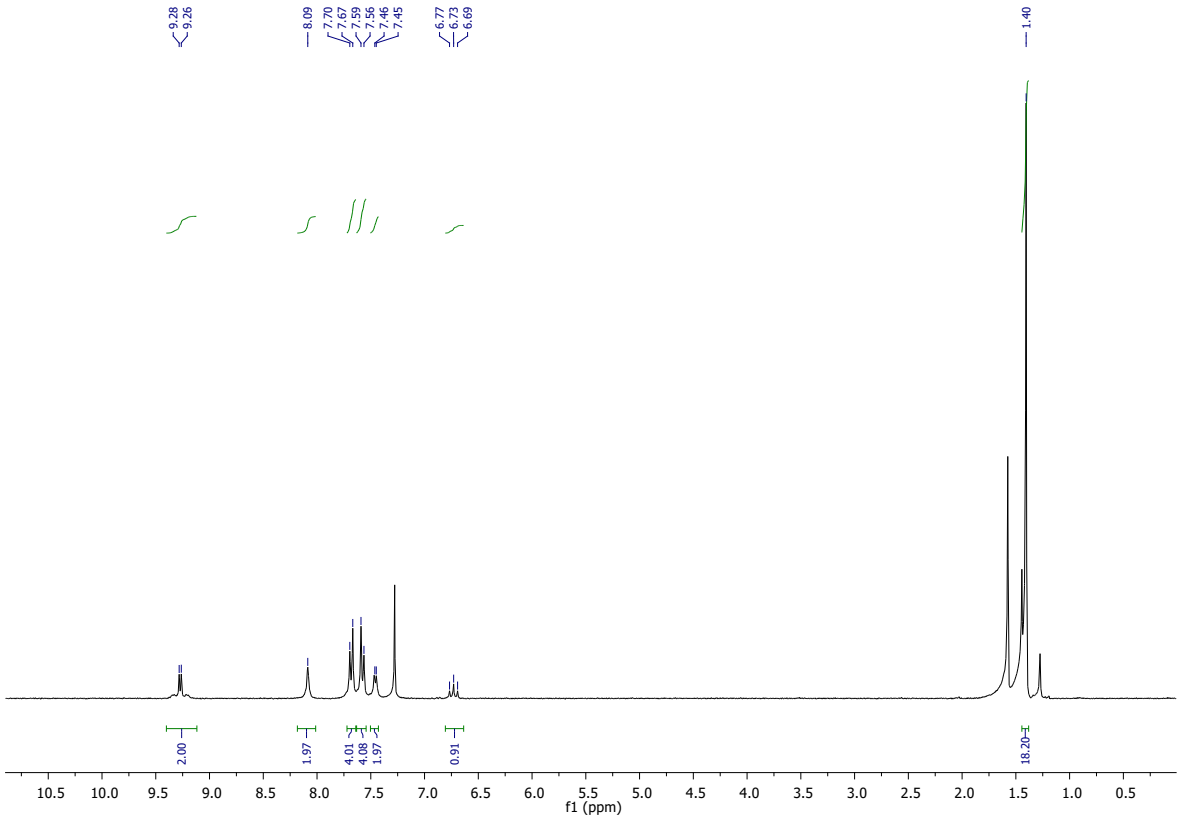

Figure S7. ^{1}H spectrum (300 MHz, $CDCl_3$) of **PtL^{3}Cl**.

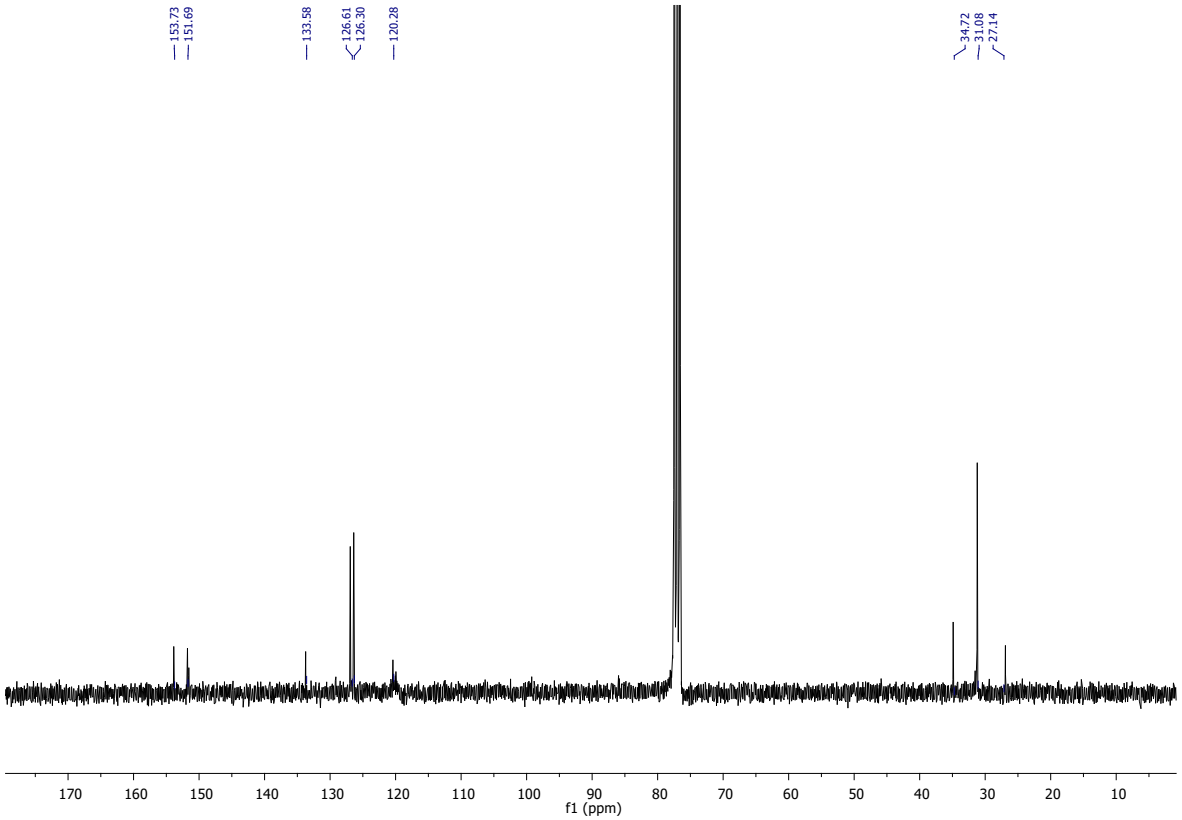

Figure S8. $^{13}C\{^{1}H\}$ spectrum (75.48 MHz, $CDCl_3$) of **PtL^{3}Cl**.

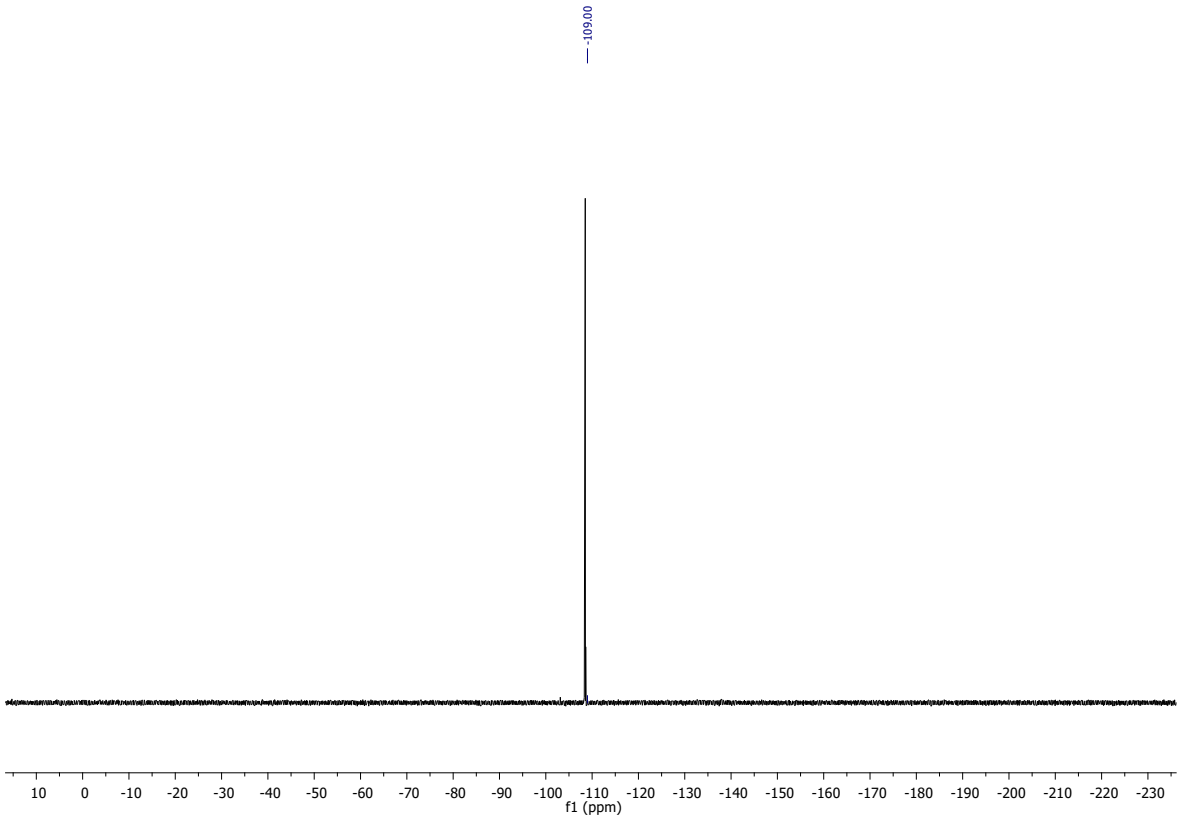

Figure S9. $^{19}F\{^{1}H\}$ spectrum (282.36 MHz, $CDCl_3$) of **PtL^{3}Cl**.

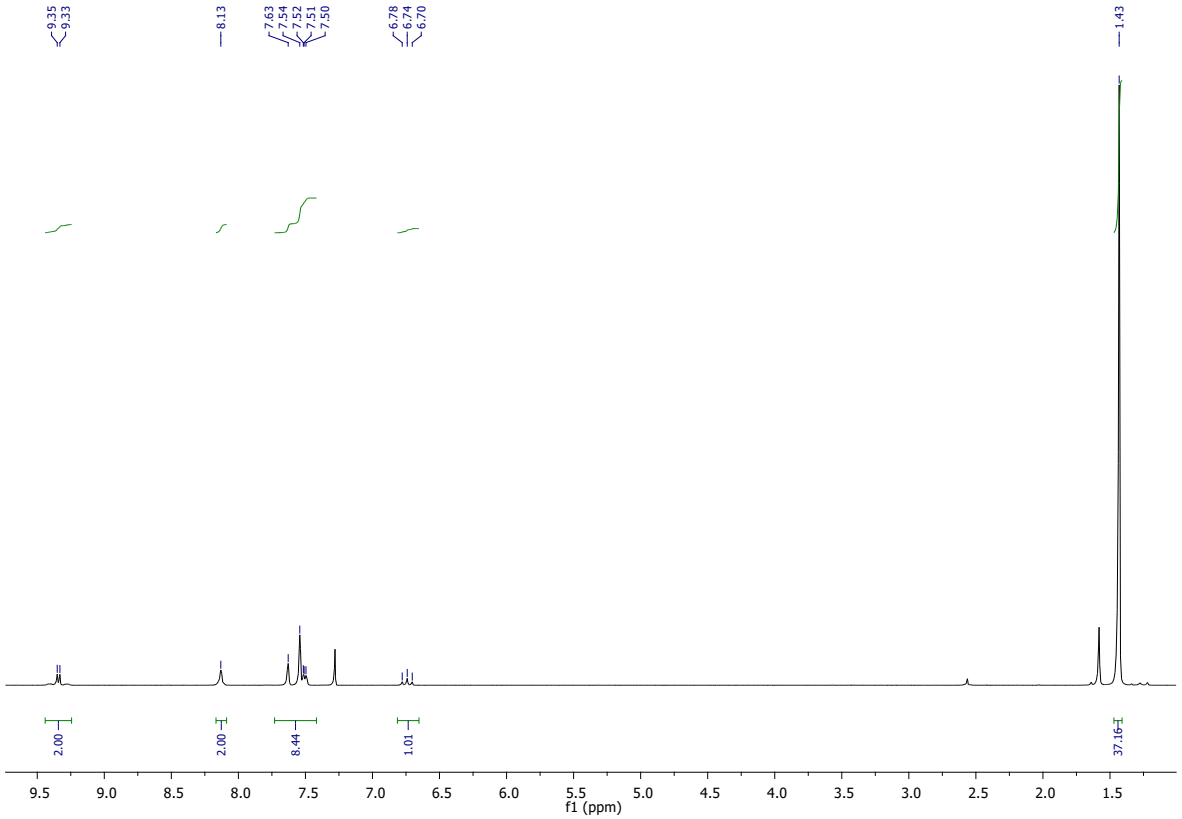

Figure S10. ^{1}H spectrum (300 MHz, $CDCl_3$) of **PtL^{4}Cl**.

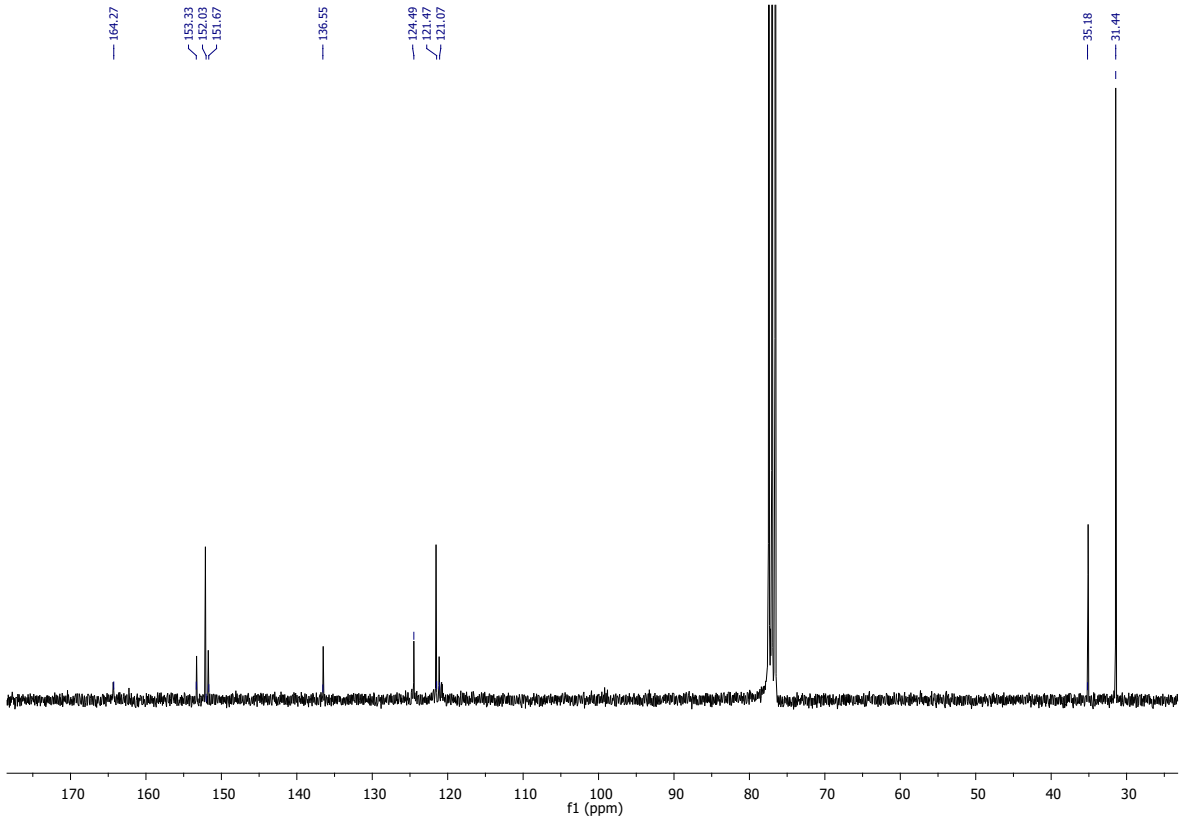

Figure S11. $^{13}C\{^{1}H\}$ spectrum (75.48 MHz, $CDCl_3$) of **PtL^{4}Cl**.

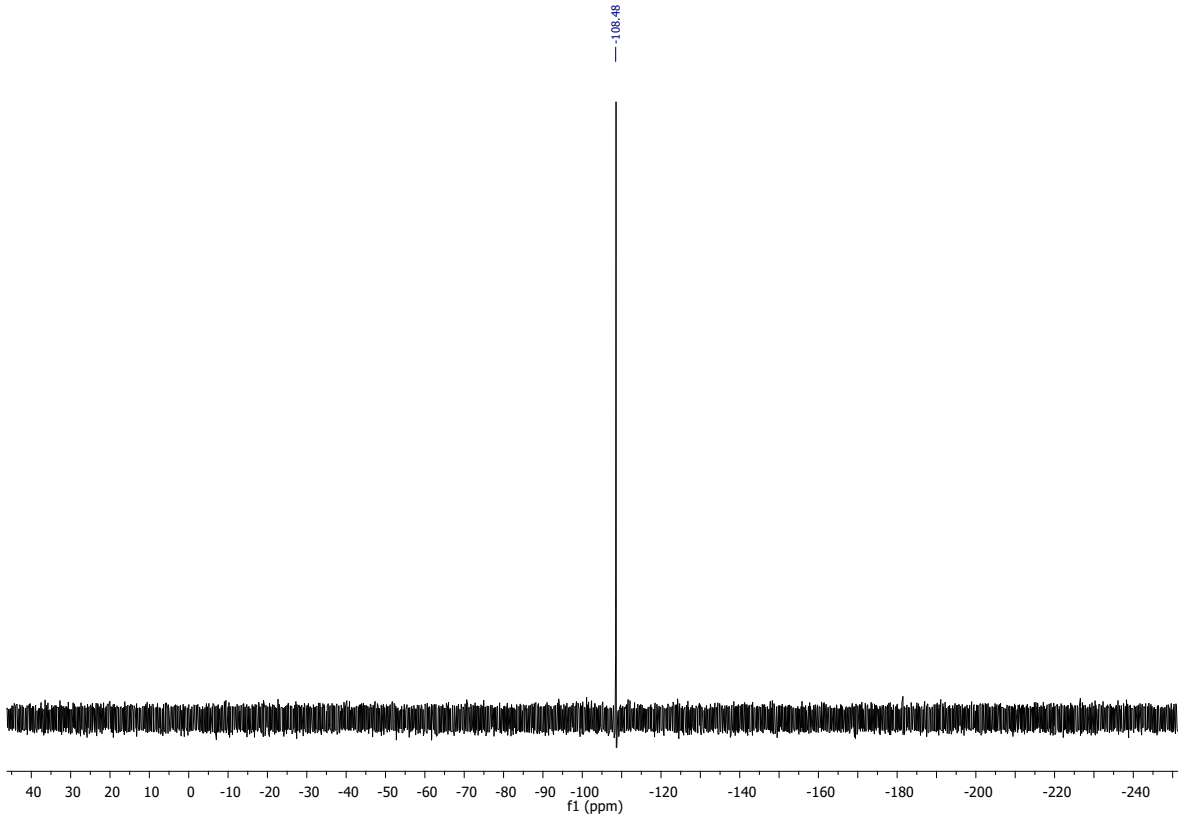

Figure S12. $^{19}F\{^{1}H\}$ spectrum (282.36 MHz, $CDCl_3$) of **PtL^{4}Cl**.

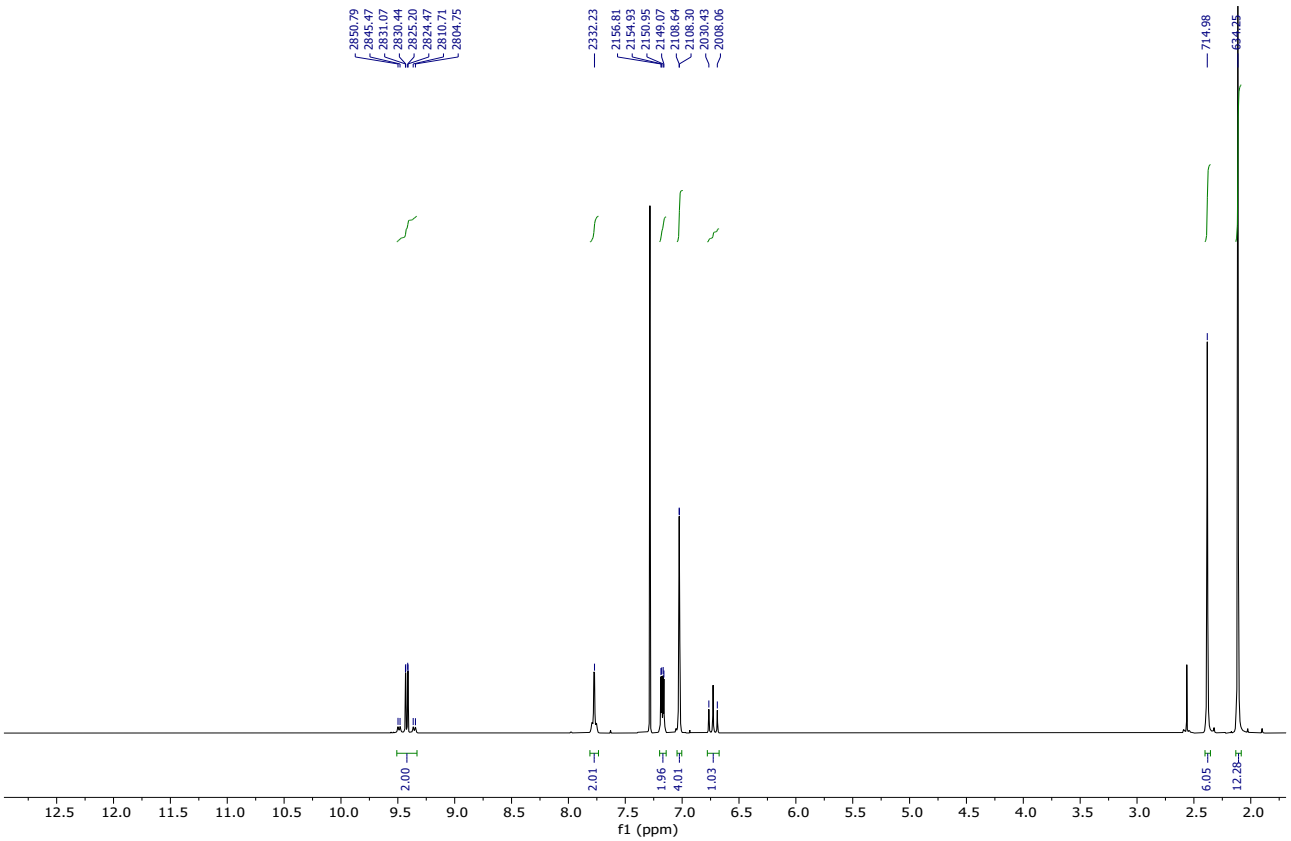

Figure S13. ^{1}H spectrum (300 MHz, $CDCl_3$) of **PtL^{5}Cl**.

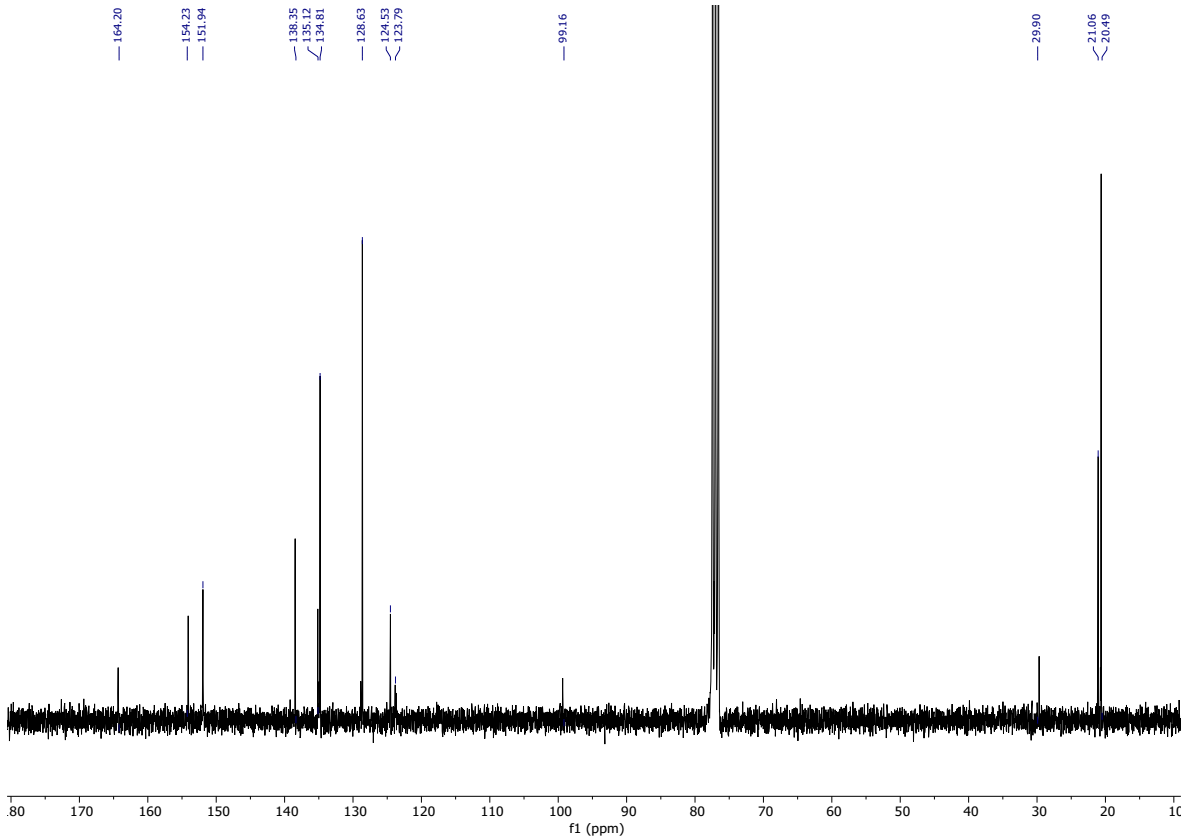

Figure S14. $^{13}C\{^{1}H\}$ spectrum (75.48 MHz, $CDCl_3$) of **PtL^{5}Cl**.

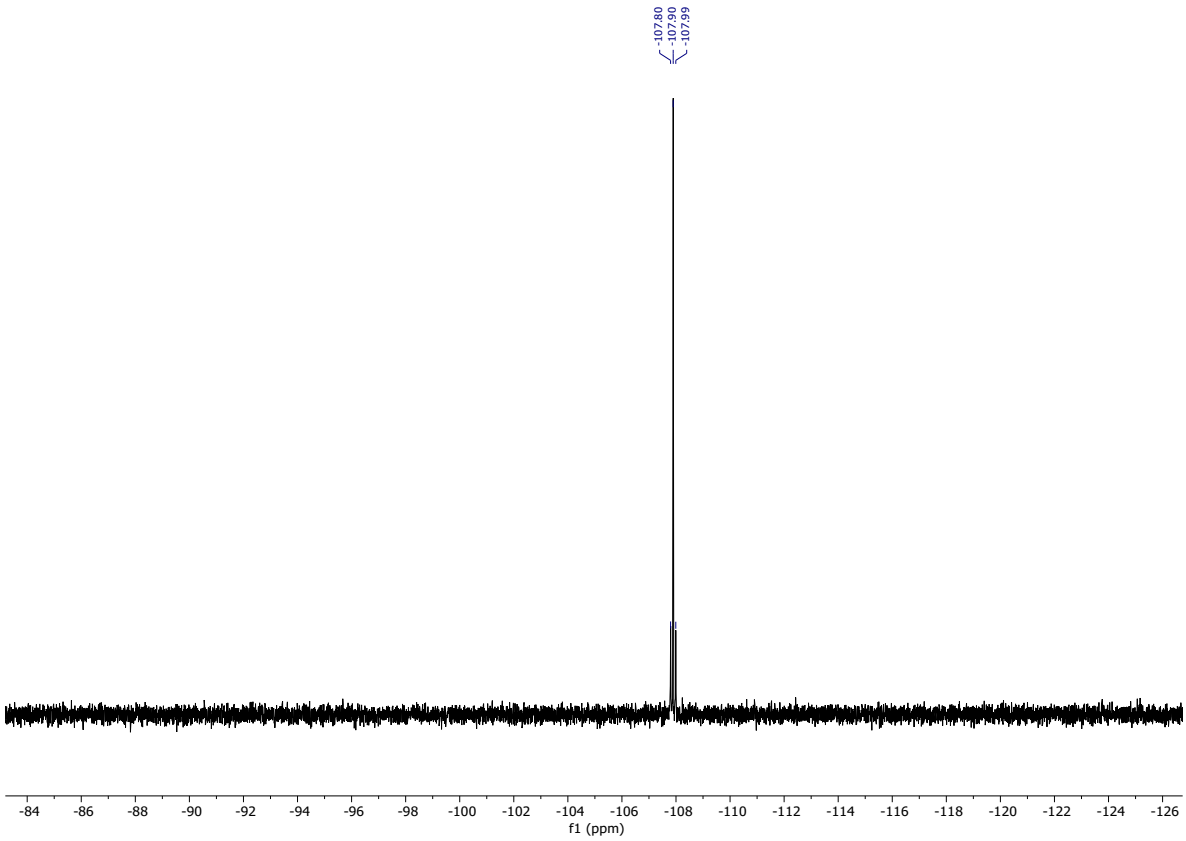

Figure S15. $^{19}F\{^{1}H\}$ spectrum (282.36 MHz, $CDCl_3$) of **PtL^{5}Cl**.

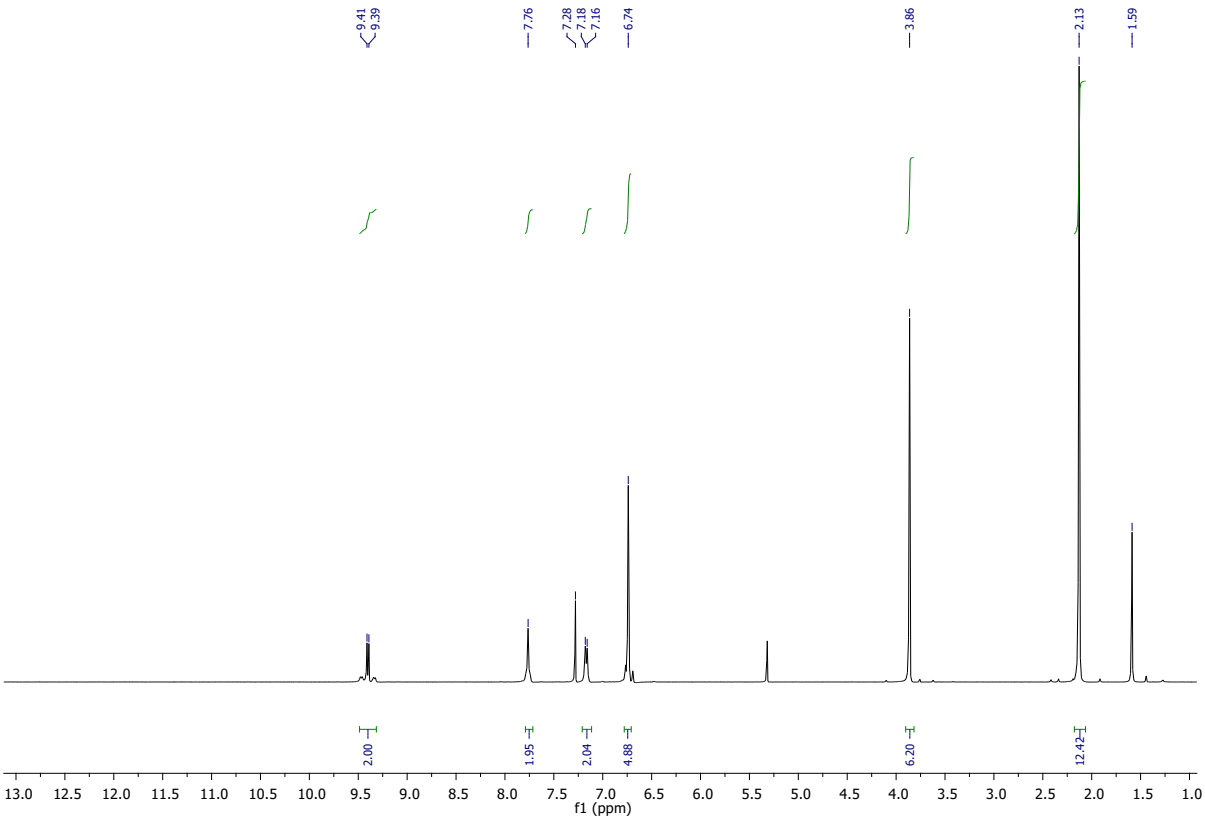

Figure S16. ^{1}H spectrum (300 MHz, $CDCl_3$) of **PtL^{6}Cl**.

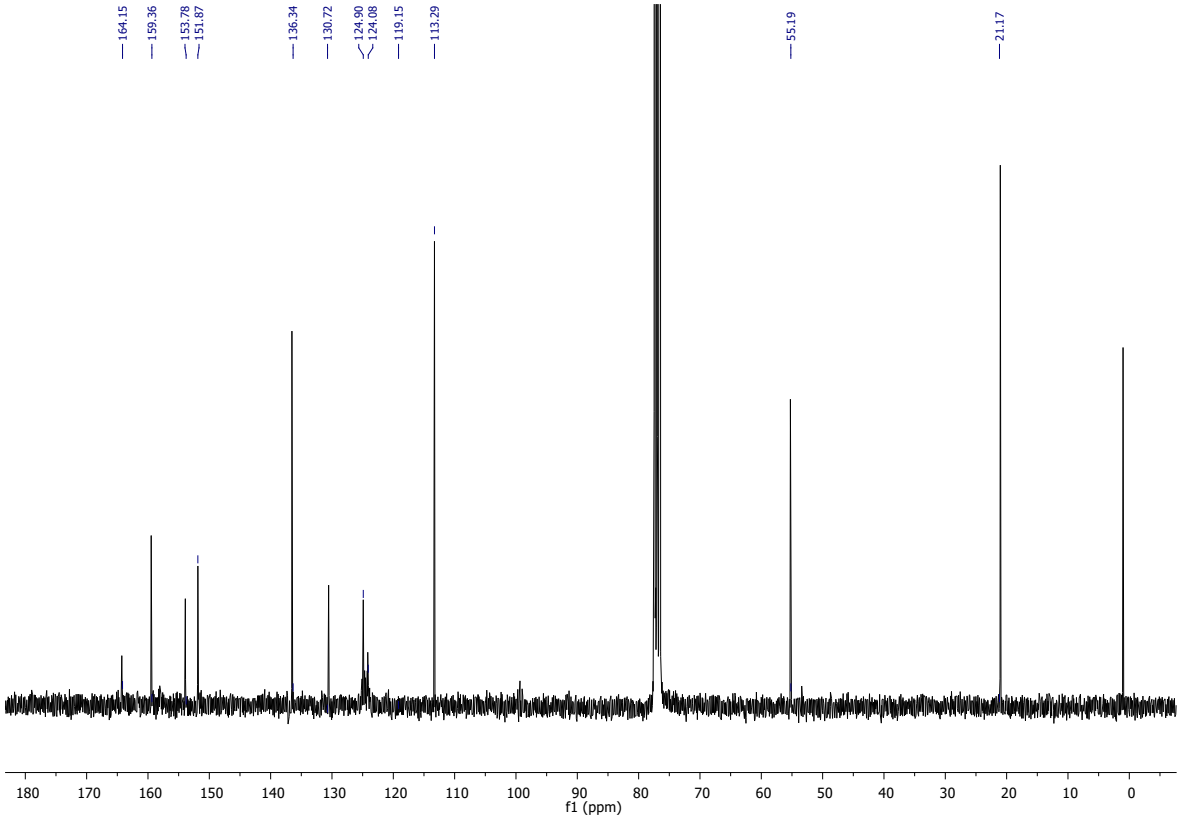

Figure S17. $^{13}C\{^{1}H\}$ spectrum (75.48 MHz, $CDCl_3$) of **PtL^{6}Cl**.

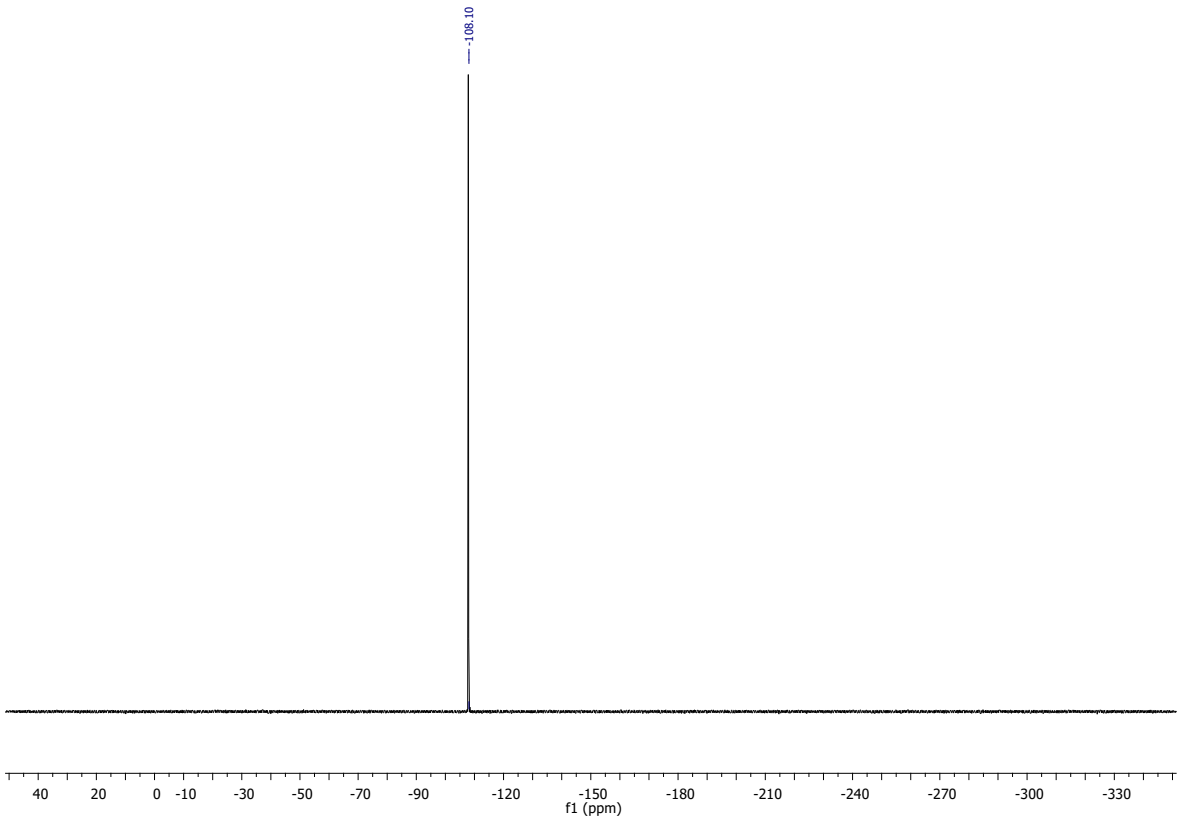

Figure S18. $^{19}F\{^{1}H\}$ spectrum (282.36 MHz, $CDCl_3$) of **PtL^{6}Cl**.

3. UV-Vis Absorption spectra of the Pt(II) complexes

UV-Visible spectra were collected by a Shimadzu UV3600 spectrophotometer, using dichloromethane as solvent and quartz cuvettes with 1 cm path length.

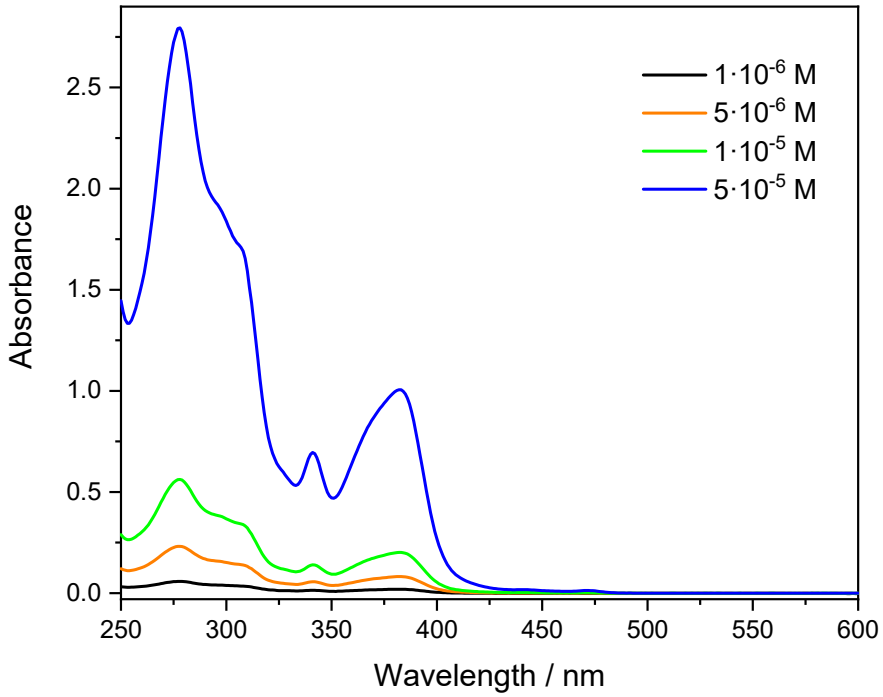

Figure S19. UV-Vis absorption spectra of **PtL^{1}Cl** at different concentrations in dichloromethane.

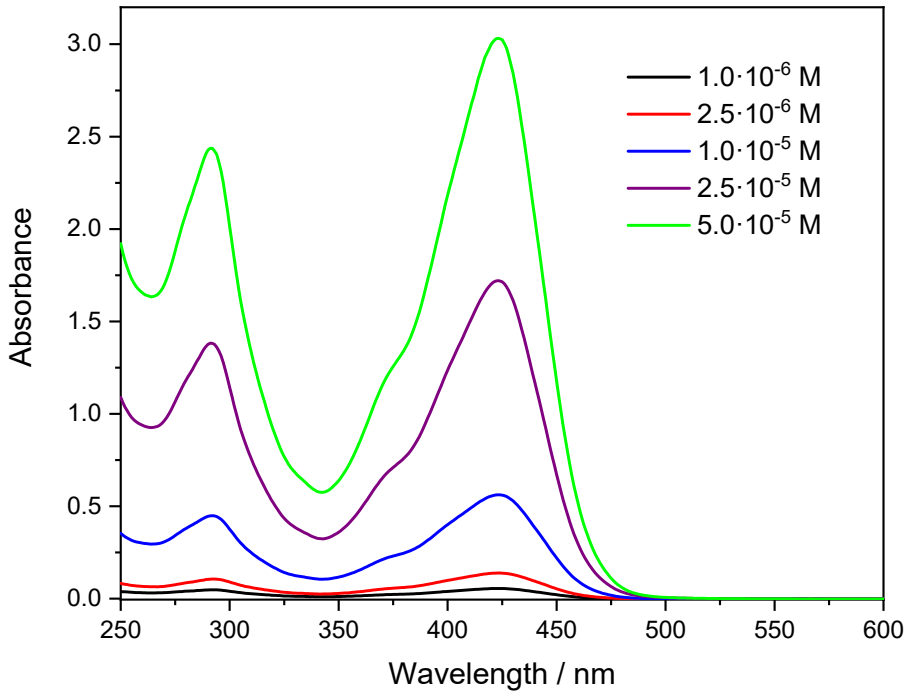

Figure S20. UV-Vis absorption spectra of **PtL^{2}Cl** at different concentrations in dichloromethane.

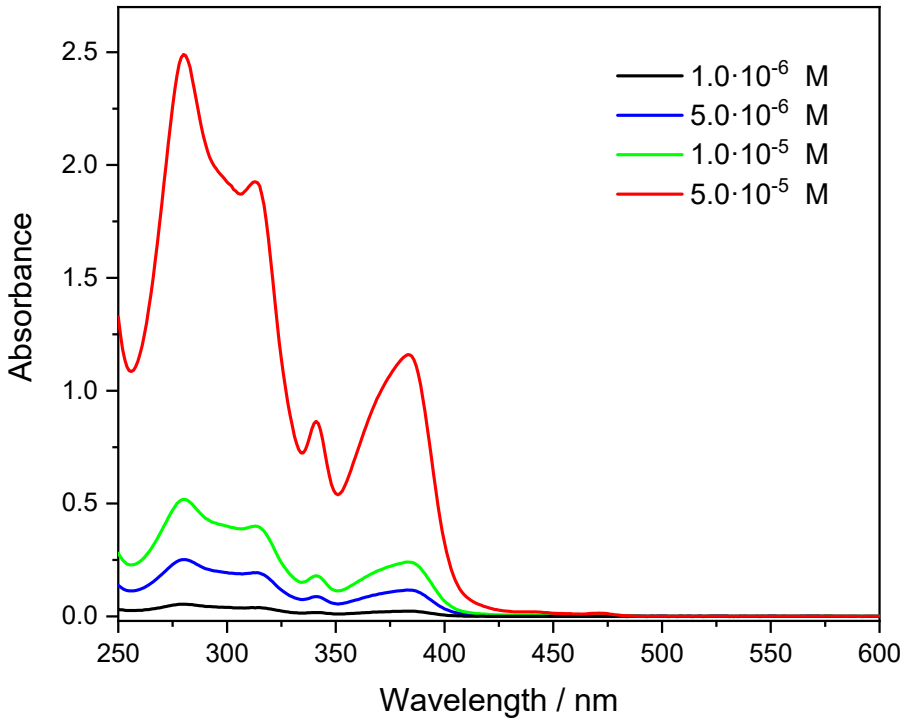

Figure S21. UV-Vis absorption spectra of **PtL^{3}Cl** at different concentrations in dichloromethane.

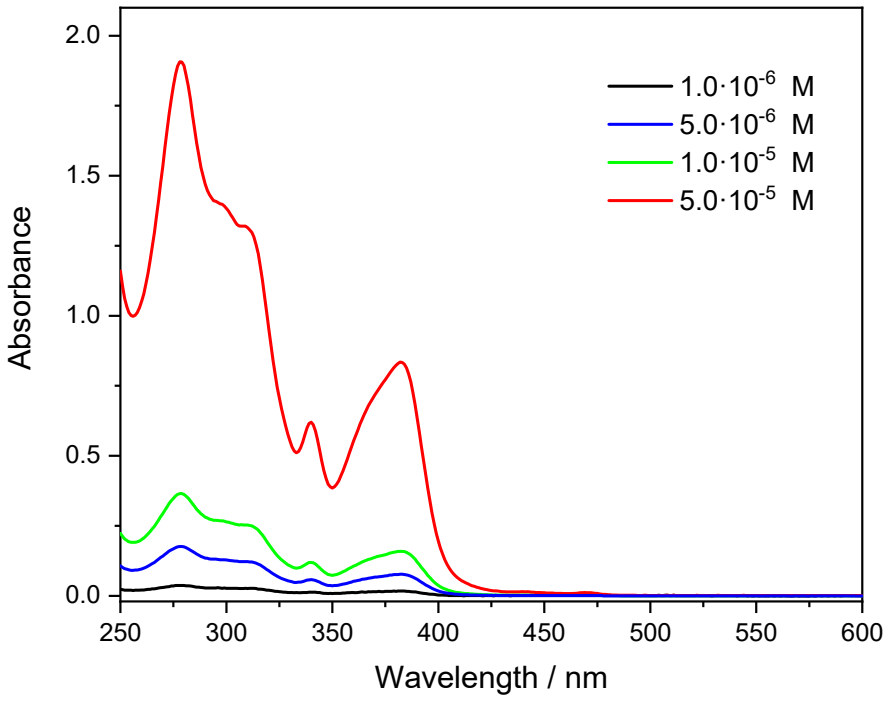

Figure S22. UV-Vis absorption spectra of **PtL^{4}Cl** at different concentrations in dichloromethane.

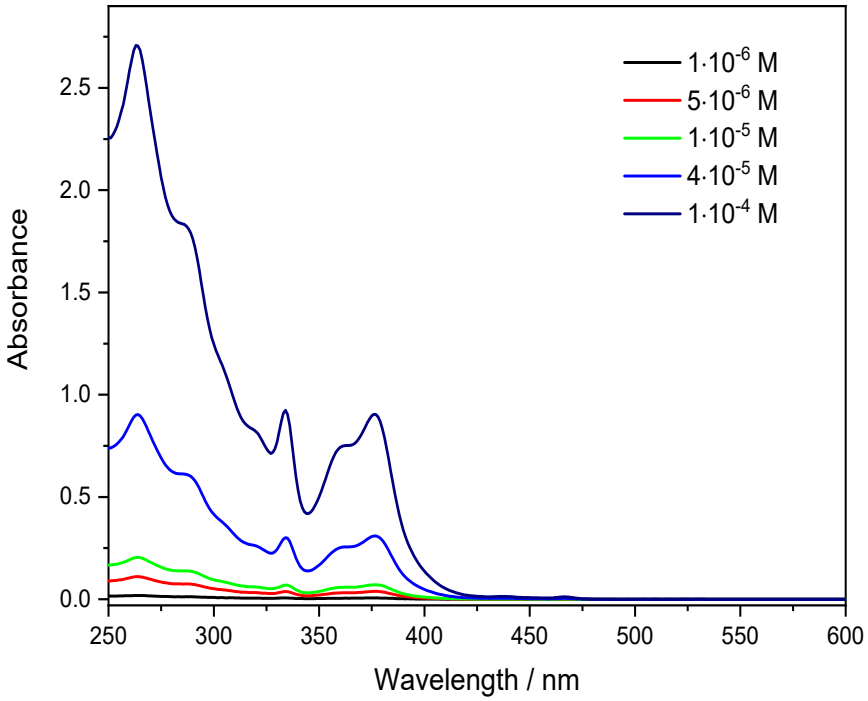

Figure S23. UV-Vis absorption spectra of **PtL^{5}Cl** at different concentrations in dichloromethane.

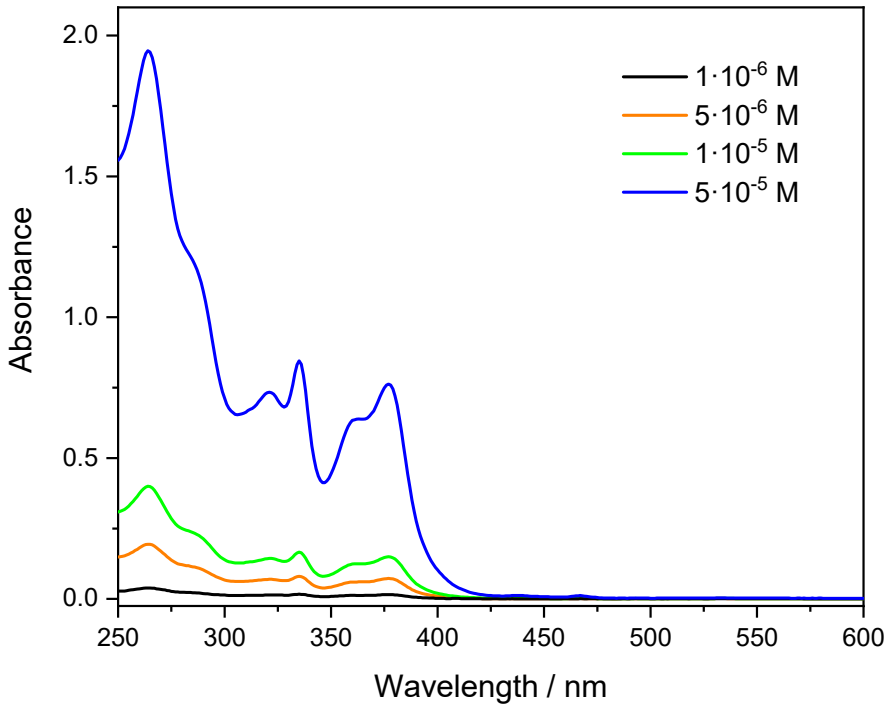

Figure S24. UV-Vis absorption spectra of **PtL^{6}Cl** at different concentrations in dichloromethane.

4. Emission spectra of the Pt(II) complexes

Measurements were carried out in dichloromethane solution after three Freeze-Pump-Thaw (FPT) cycles, necessary to remove dissolved oxygen. Emission spectra were collected by a FLS980 spectrofluorimeter (Edinburg Instrument Ltd).

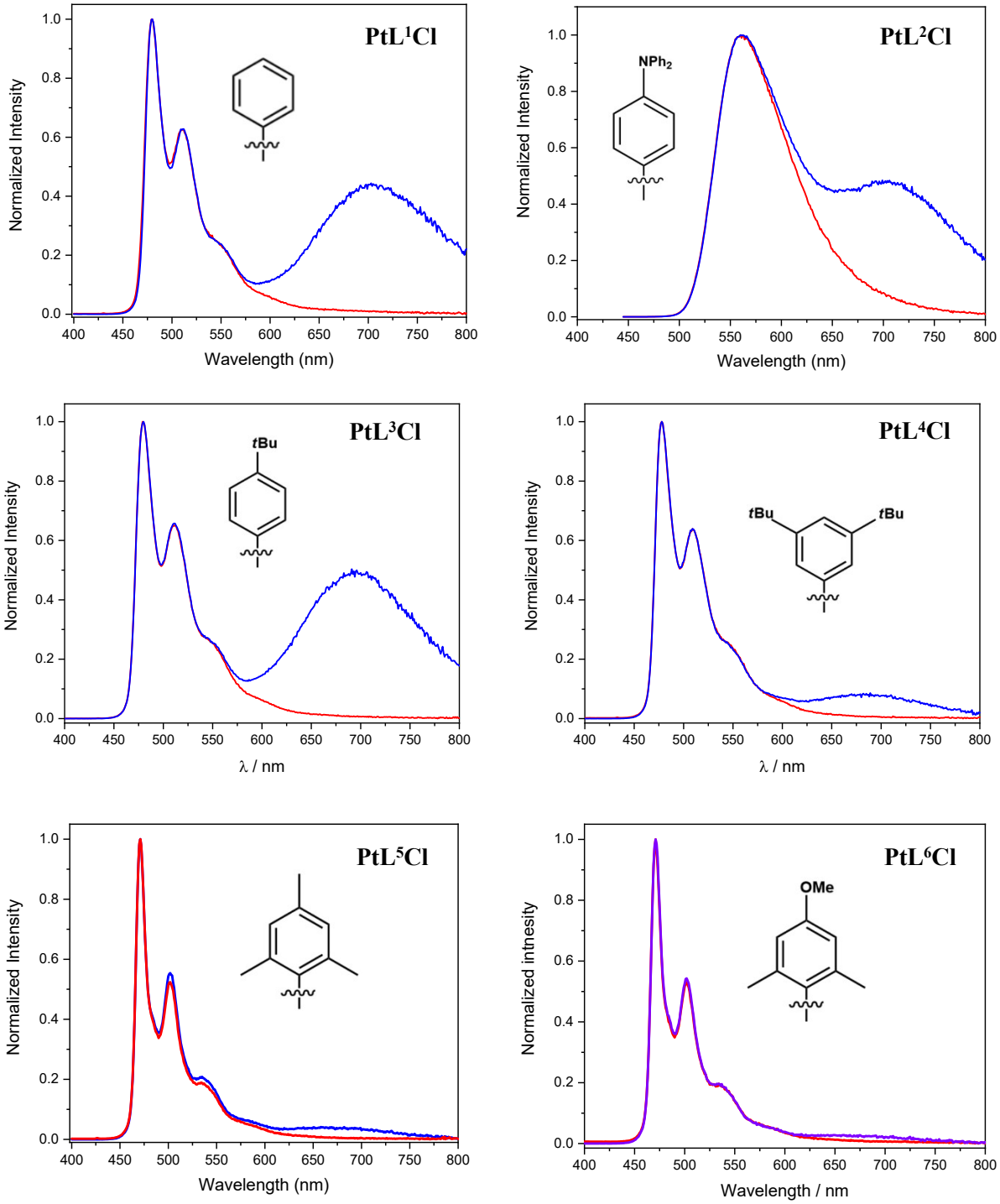

Figure S25. Normalized emission spectra of complexes **PtL¹Cl-PtL⁶Cl** in dilute ($5.0 \cdot 10^{-6}$ M, red) and concentrated ($2.0 \cdot 10^{-4}$ M, blue) dichloromethane solution at 298 K after the FPT cycles.

5. Lifetime measurements

Measurements were carried out in dichloromethane solution after three Freeze-Pump-Thaw (FPT) cycles, necessary to remove dissolved oxygen. Emission spectra were collected by a FLS980 spectrofluorimeter (Edinburg Instrument Ltd).

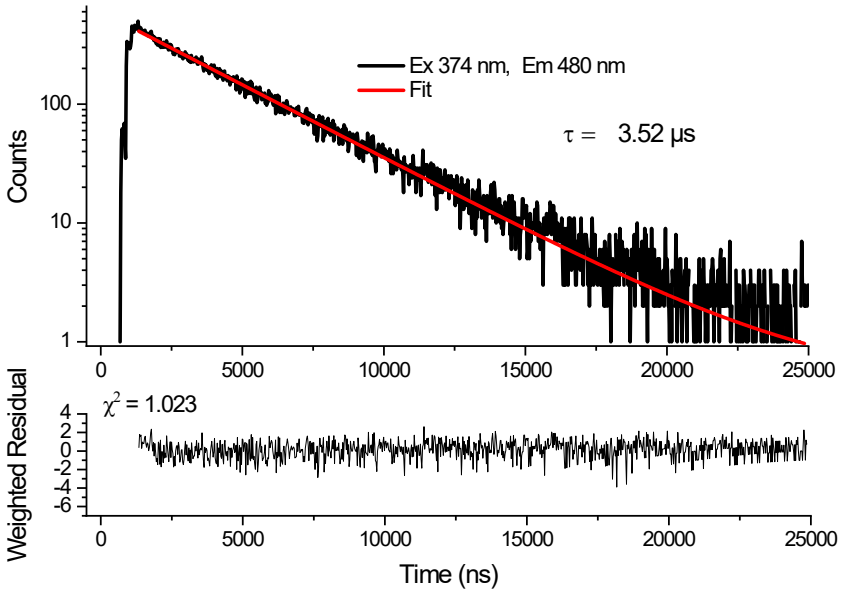

Figure S26. Excited state decay of complex **PtL^{1}Cl** in dilute ($5.0 \cdot 10^{-6}$ M) dichloromethane solution at 298 K after the FPT cycles.

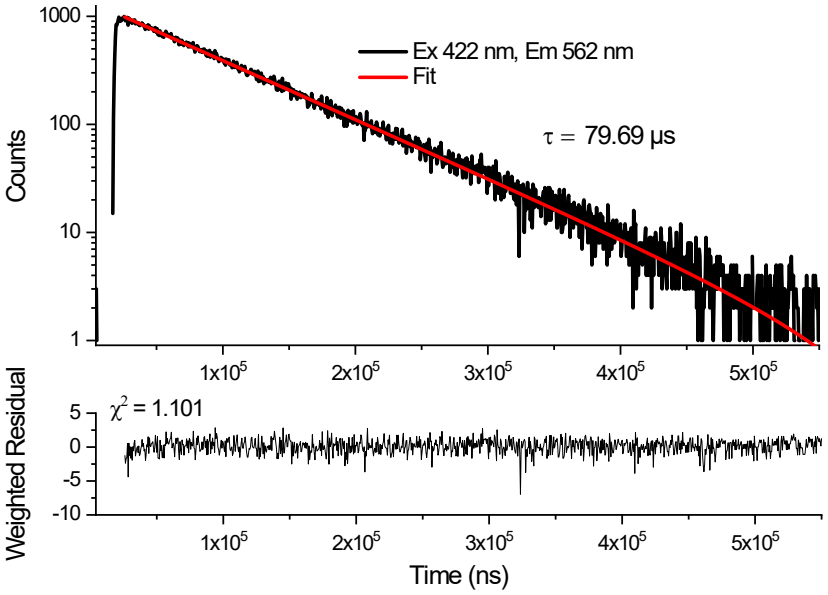

Figure S27. Excited state decay of complex **PtL^{2}Cl** in dilute ($5.0 \cdot 10^{-6}$ M) dichloromethane solution at 298 K after the FPT cycles.

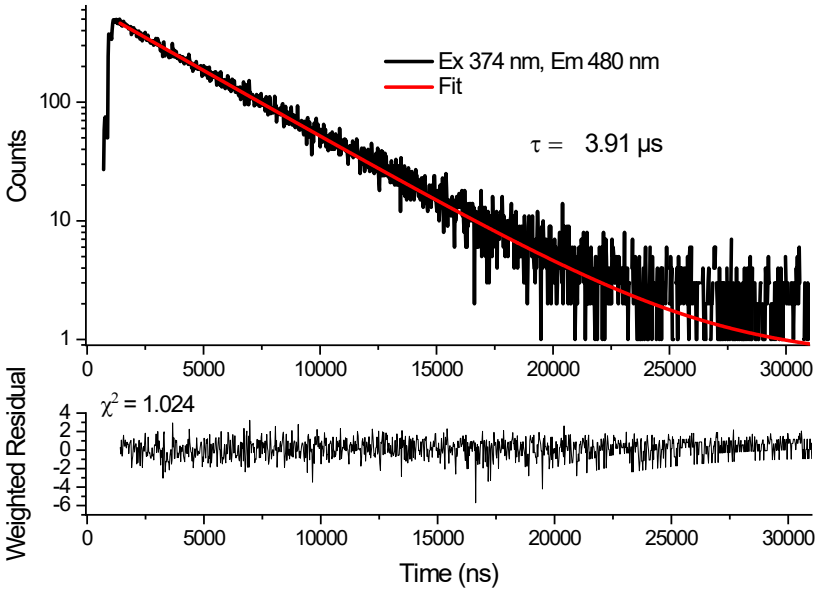

Figure S28. Excited state decay of complex **PtL^{3}Cl** in dilute ($5.0 \cdot 10^{-6}$ M) dichloromethane solution at 298 K after the FPT cycles.

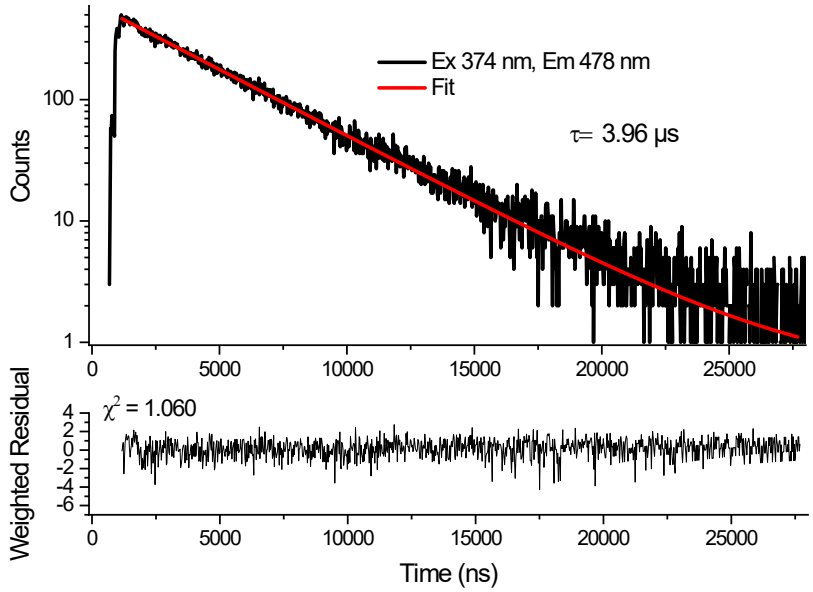

Figure S29. Excited state decay of complex **PtL^{4}Cl** in dilute ($5.0 \cdot 10^{-6}$ M) dichloromethane solution at 298 K after the FPT cycles.

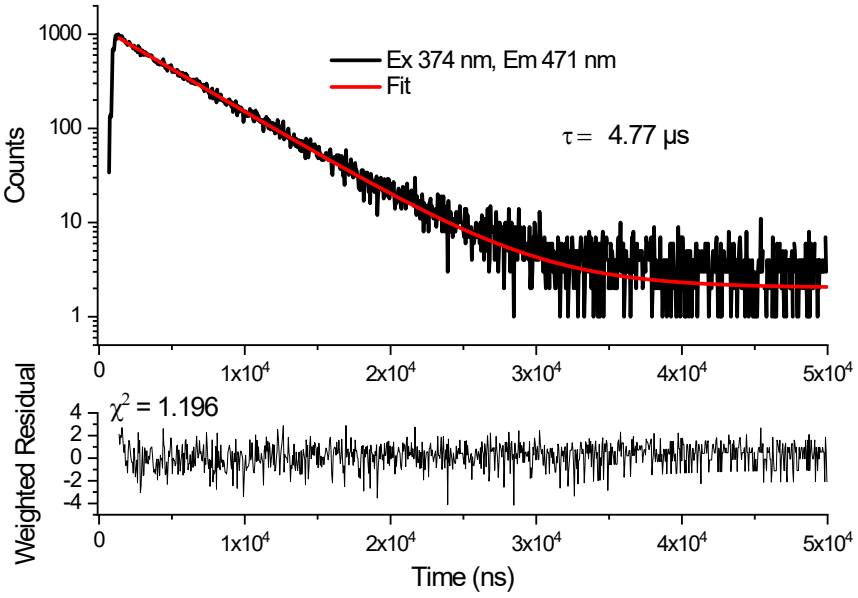

Figure S30. Excited state decay of complex **PtL^{5}Cl** in dilute ($5.0 \cdot 10^{-6}$ M) dichloromethane solution at 298 K after the FPT cycles.

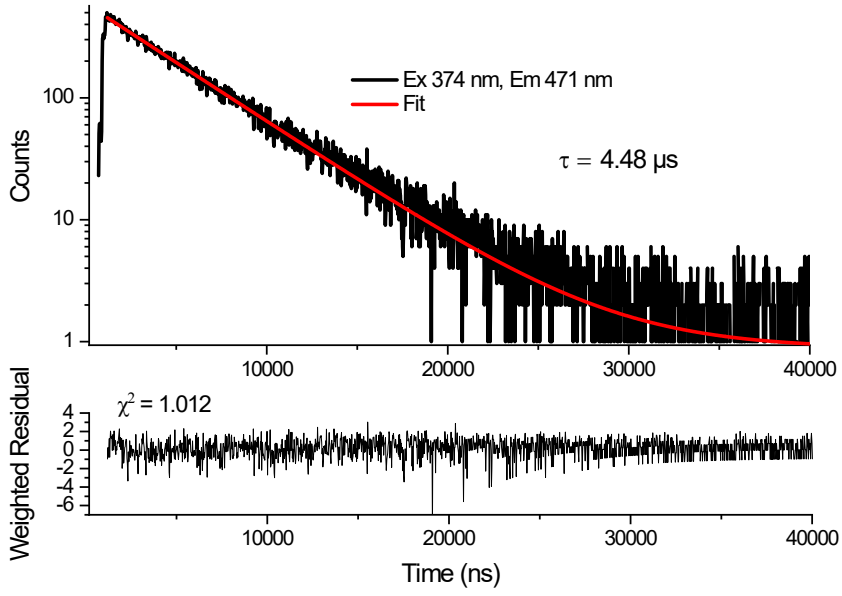

Figure S31. Excited state decay of complex **PtL^{6}Cl** in dilute ($5.0 \cdot 10^{-6}$ M) dichloromethane solution at 298 K after the FPT cycles.

6. OLEDs fabrication

OLEDs were fabricated by growing a sequence of thin layers on clean glass substrates pre-coated with a 120 nm-thick layer of indium tin oxide (ITO) with a sheet resistance of 20 U per square. A 2 nm-thick hole-injecting layer of MoOx was deposited on top of the ITO by thermal evaporation under high vacuum of 10^{-6} hPa. The other layers were deposited in succession by thermal evaporation under high vacuum: first, 4,4',4''-tris(N-carbazolyl)triphenylamine (50 nm) as exciton blocking layers; second, the emitting layer evaporated by co-deposition of the suitable platinum complex and (bis-4-(N-carbazolyl)phenyl)phenylphosphine oxide (BCPO) to form a 30 nm-thick blend film (6 wt% Pt complex : 94 wt% BCPO), or by single deposition of the pure platinum complex, to form a 30 nm neat film; third, 2,2',2"-(1,3,5-benzinetriyl)-tris(1-phenyl-1-H-benzimidazole (30 nm) as an electron-transporting and hole-blocking layer. This was followed by thermal evaporation of the cathode layer consisting of 0.5 nm thick LiF and a 100 nm thick aluminium cap.

The current–voltage characteristics were measured with a Keithley Source-Measure unit, model 236, under continuous operation mode, while the light output power was measured with an EG&G power meter, and electroluminescence (EL) spectra recorded with a StellarNet spectroradiometer. All measurements were carried out at room temperature under argon atmosphere and were reproduced for five runs, excluding any irreversible chemical and morphological changes in the devices.

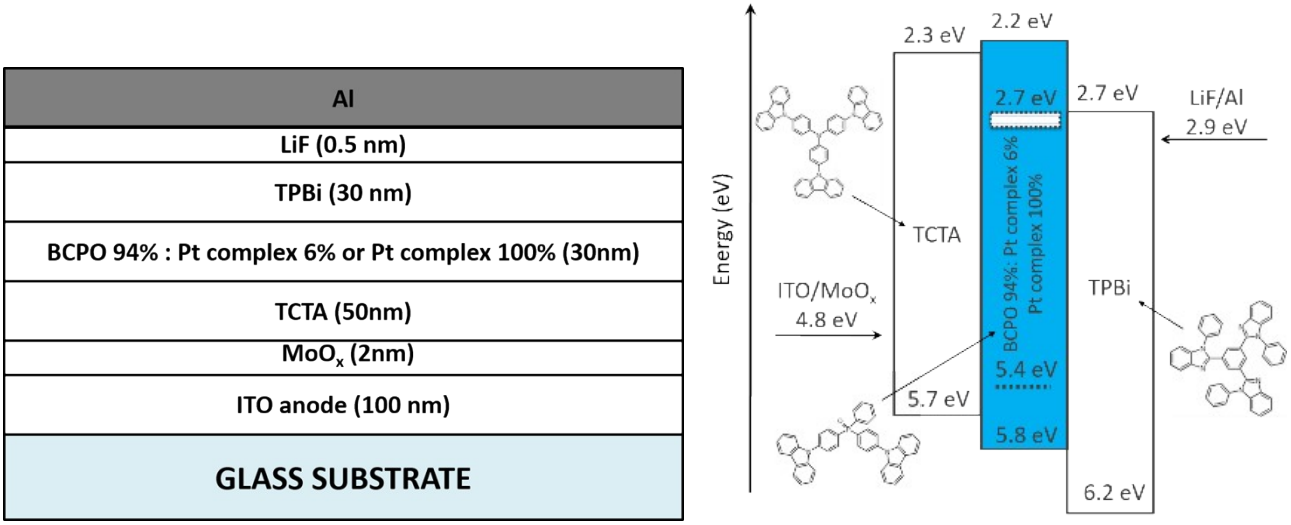

Figure S32. OLED structure (left) and energy level diagram (right).